Time-Varying Equivalent Roll Damping Coefficient and Natural Frequency Estimation via Augmented Extended Kalman Filtering for Floating Body

Yavuz Hakan Ozdemir*

Canakkale Onsekiz Mart University, Department of Motor Vehicles and Transportation Technologies Canakkale, Turkey, email: yhozdemir@comu.edu.tr, phone: +90-286-29341/5107, mobile phone: +90-5334606098, fax: +90-218-3317

Corresponding Author: Yavuz Hakan Ozdemir

Time-Varying Equivalent Roll Damping Coefficient and Natural Frequency Estimation via Augmented Extended Kalman Filtering for Floating Body

The time-varying equivalent roll damping coefficient and natural frequency in a nonlinear state-space model of a floating body are discussed in this article using an augmented extended Kalman filtering (EKF) method. In this paper, we present an estimation technique that can identify changes in the damping properties of the system considered by a single parameter based on roll angle data. The model used an augmented EKF to overcome parameter variability and noisy measurement input. The calculated error was compared with the covariance matrix's theoretical restrictions to determine whether the filtering was effective. It is found that the equivalent damping coefficient and natural frequency obtained from the EKF method is a more accurate depiction of the roll dynamics from the general estimation procedure given by the literature. The suggested technique has the ability to eliminate random noise from the measured signal. The effect of measurement noise levels on identification accuracy was investigated and discussed.

Keywords: Extended Kalman filter, system identification, equivalent damping coefficient, parameter estimation, roll damping, natural frequency

1. Introduction

1.1. Background

Establishing hydrodynamic loads and assessing structural responses are pivotal elements within a robust design procedure for ships and offshore structures. In the design phase, it is advisable to model the rolling behavior of a hull form, including the associated parameters such as damping coefficient and natural frequency. In terms of ship safety at sea, rolling is still a serious occurrence. Excessive amplitude in rolling motion will negatively affect ship stability. In such cases, either the form should be redesigned, or efforts should be made to reduce the amplitude of the rolling motion with the help of a controller. Determining the internal states of a dynamic system is essential for effective control. To design a robust controller, one must understand both the governing equation of the system and the associated parameters and states. Calculating roll-damping coefficients and natural frequency has been an active research topic for years, and in this study, the calculation method of the roll-damping coefficient and natural frequency with the extended Kalman filter was examined.

1.2. Formulation of the Problem

The basic 1DoF equation below describes the non-linear roll damping of a ship's roll decay motion:

$$\left(\mathrm{I}+\mathrm{A}\right)\ddot{\phi}+\mathrm{B}_{\phi}\left(\dot{\phi}\right)+\mathrm{C}_{\phi}\phi=0, \tag{1}$$

where $\mathrm{B}_{\phi}\left(\dot{\phi}\right)$ stands for nonlinear roll damping moment (*Nms*), I is the roll mass moment of inertia (*kgm*^{2}), and A is the added mass moment of inertia (*kgm*^{2}). The roll angle, angular velocity, and angular acceleration are denoted, respectively, as $\phi, \dot{\phi}$ and $\ddot{\phi}$ [1].

A series expansion with a linear component and higher-order nonlinear terms, as a function of ϕ and $\dot{\phi}$, can be used to describe the nonlinear damping moment B_{ϕ} [1]:

$$\mathrm{B}_{\phi}=\mathrm{B}_{\phi 1}\dot{\phi}+\mathrm{B}_{\phi 2}\dot{\phi}\left|\dot{\phi}\right|+\mathrm{B}_{\phi 3}\dot{\phi}^{3}+\cdots, \tag{2}$$

this refers to a model with nonlinearity. By substituting Eq. (2) into Eq. (1) for the calm water roll decay test, the equation of motion transforms to:

$$\left(\mathrm{I}+\mathrm{A}\right)\ddot{\phi}+\mathrm{B}_{\phi 1}\dot{\phi}+\mathrm{B}_{\phi 2}\dot{\phi}\left|\dot{\phi}\right|+\mathrm{B}_{\phi 3}\dot{\phi}^{3}+\mathrm{C}_{\phi}\phi=0. \tag{3}$$

Equation (3) can be reformulated more conventionally using the acceleration coefficients, following the nomenclature outlined in ITTC-Recommended Procedures and Guidelines, [1]:

$$\ddot{\phi}+2\alpha\dot{\phi}+\beta\dot{\phi}\left|\dot{\phi}\right|+\gamma\dot{\phi}^{3}+\omega_{\phi}^{2}\phi=0, \tag{4}$$

where:

$$2\alpha = \frac{B_{\phi 1}}{I+A},\ \beta = \frac{B_{\phi 2}}{I+A},\ \gamma = \frac{B_{\phi 3}}{I+A},\ \omega_\phi = \sqrt{\frac{C_\phi}{I+A}} = \frac{2\pi}{T_\phi}. \quad (5)$$

in Eq. (4), the quantity ω_ϕ denotes the natural frequency. The linearized roll decay motion with an equivalent damping coefficient is:

$$\ddot{\phi} + \alpha_E \dot{\phi} + \omega_\phi^2 \phi = 0. \quad (6)$$

Corresponding to Eq. (4), an equivalent damping coefficient α_E can be defined as:

$$\alpha_E = 2\alpha + \frac{8}{3\pi}\omega\phi_i\beta + \frac{3}{4}\omega^2\phi_i^2\gamma, \quad (7)$$

Where ϕ_i is the amplitude of the i-th oscillation cycle and ω is the oscillation frequency in the i-th cycle [2].

A roll decay test is the most effective method for determining the equivalent damping coefficient because of how easily it can be implemented. Additionally, the International Maritime Organization (IMO) has recommended this course of action [3].

Following the experimentally or numerically simulated roll decay test, the recorded roll motion is utilized to compute the roll damping coefficients through the analysis of time series data of roll angles. Simultaneously computing the α_E and ω_ϕ values as outlined in Eq. 6 through time series data proves to be a challenge. The presence of measurement noise in experimental studies introduces complexity to the resolution of this problem.

Eq. (4) was solved by the fourth-order Runge-Kutta method and the validity of the model was checked.

1.3. Literature Survey

Several researchers describe some techniques for calculating roll damping coefficients in depth.

While Ikeda et. al [4] have developed an empirical method to evaluate roll damping, pioneering studies conducted by Froude [5], Himeno [6], and Spouge [7] were presented to precisely assess the roll damping coefficients based on the resulting peak values of the roll angle from roll decay tests.

The roll decay test can be used to calculate the damping coefficients for vessel roll motion in five different ways [7]: The Froude Energy technique, the Roberts Energy method, the Averaging approach, the Perturbation method, and the quasi-linear method. In recent times, thorough literature reviews on various approaches for estimating roll damping in floating

bodies have been presented by Igbadumhe et. al [3], Wassermann et. al [8], Yu et. al [9], Manderbacka et. al [10] and Rodríguez et. al [11].

The usefulness of these methods has been limited to a few straightforward models, like linear-plus-quadratic and linear-plus-cubic [12]. It is challenging to calculate both α_E and ω_ϕ simultaneously, as seen in Eq. 6. Consequently, in the methods found in the literature, the natural frequency (ω_ϕ) is often assumed to be identical to the damped frequency (ω). The parameter α_E varies with time, and existing methods in the literature are unable to calculate its time-dependent changes [13]. Moreover, measurement noise presents a major problem in experiments. Most notably, these methods can only be applied to equations with one degree of freedom (1DOF). Despite their disadvantages, these methods continue to be employed today for evaluating the results of both experimental and numerical studies to obtain roll damping [11], [14-16].

The well-known Kalman filter, introduced by Kalman and Bucy [17], stands as one of the most significant algorithms for estimating the state of a system. Under the considerations of a linear model, it provides the optimal solution for minimizing mean square estimation error. However, when dealing with nonlinear filters, analytical solutions become challenging, necessitating the use of estimators, as noted by Welch and Bishop [18], Reina et. al [19].

The EKF technique has been widely employed in various industrial applications of the engineering disciplines for parameter estimation and system modelling. For instance, several aircraft aerodynamic parameter estimation issues have been effectively solved using the EKF. Chowdhary and Jategaonkar [20] presented parameter estimation techniques dependent on Kalman filters' use of aircraft flight data. Their findings show that the EKF algorithm is still a useful device for identifying flight system parameters. Megyesi et. al [21] employed an optimal Kalman filter that allows the determination of the optimal output signal. In their study, process, and measurement noise for different unmanned aerial vehicle speeds was effectively reduced. A practical EKF-based error filtering method for a nonlinear dynamic system with process and measurement noise was extended by Wang et. al [22], Wang et. al while [23] proposed an aircraft Anti-lock Braking System (ABS) control technique based on EKF. The success of the suggested control technique was confirmed through both simulation and experimental analyses. Furthermore, the Kalman filter has been utilized in structural engineering because of its relative simplicity.

Zhi et. al [24] employed the Extended Kalman Filter (EKF) method to assess wind loads on a towering skyscraper, while Wu et. al [25] applied the Unscented Kalman Filter (UKF) method

to estimate aerodynamic damping. Additionally, Yang et. al [26] introduced a Kalman filter-based method for inverting wind loads on tall buildings. In another study, Song et. al [27] presented adaptive Kalman filters for nonlinear model updating of the building structure.

The EKF is also a widely used real-time observation problem-solving tool with a wide range of automotive applications. A novel approach to the issue of suspension system state estimation utilizing a Kalman Filter (KF) under diverse road conditions is presented by Wang et. al [23]. Their findings demonstrate that the suggested method can estimate a suspension system's state with a high degree of accuracy. In order to predict the road profiles travelled by a certain vehicle from the dynamic responses observed on this vehicle, Fauriat et. al [28] developed a data processing approach based on the Kalman filter. In order to deal with model parameter fluctuation and noisy measurement input, Reina and Messina [29] introduced a non-linear model-based observer that uses an augmented Extended Kalman filter. To predict several vehicle key states, Liu et. al [30] suggested a hybrid approach that combines an unscented Kalman filter (UKF) and a genetic-particle swarm algorithm (genetic-particle swarm UKF). For vehicle dynamics, Rodriguez et. al [31] presented a novel accurate estimator that is a new kind of dual Kalman filter. Results demonstrate that the novel observer accurately predicts the important factors for vehicle dynamics. Xu et. al [32] developed and validated a localization algorithm, which uses error-state Kalman filtering for deep-sea mining vehicles.

1.4. Scope of this study

The scope of this study is to develop an enhanced inverse method based on the extended Kalman filter (EKF) for estimating the time-varying linear equivalent damping coefficient and natural frequency using data obtained from roll decay tests. This is the first time, to the best of the author's knowledge, that a method like this has been systematically employed for estimating states and identifying parameters in roll decay motion. The purpose of this investigation is to simultaneously estimate α_E and ω_ϕ by mitigating the measurement noise at the system output using the EKF and to observe the change of α_E over time. This study aims, importantly, to introduce a method applicable to motions with high degrees of freedom. The performance of an EKF approach will be assessed using numerical examples in this research. We put the technique to the test with the DTMB 5512 hull parameters, which have a wide range of both experimental and computational results in the literature. This study's major

novelty is demonstrating how this method can be used for hydrodynamic parameter identification and state estimation.

1.5 Organization of the paper

The structure of this paper is as follows: Section 2 presents the equation of roll decay coefficients and details of the pseudo-experiment. Brief explanations of the EKF method are provided in Section 3, and Section 4 presents the initial estimation error and model error of the EKF. The results are discussed in Section 5, followed by a detailed explanation of the study's contribution to the literature in Section 6 based on the obtained results. Finally, the conclusion is presented in Section 7.

2. Experimental values

The process of data assimilation requires experimental values. In this study, pseudo-experimental values were created instead of conducting the actual experiment. We tested the technique using the DTMB 5512 hull parameters, which have been the subject of numerous experimental and computational studies in the literature. Subsequently, these parameters are treated as unknowns and determined during the estimation stage.

2.1. Decay coefficient

In a free-roll test, the ship is heeled to the desired angle and then released. The absolute value of the roll angle at the moment of the n-th peak value is shown by the symbol ϕ_i, which can be seen in Figure 1 typical roll decay curve. The so-called decay curve explains how ϕ_i decreases as a function of the mean roll angle. A third-degree polynomial is used to match the decay curve [1,2]:

$$\Delta\phi = a\phi_m + b\phi_m^2 + c\phi_m^3, \tag{8}$$

where:

$$\Delta\phi = \phi_{i-1} - \phi_i, \tag{9}$$

$$\phi_m = \left(\phi_{i-1} + \phi_i\right)/2. \tag{10}$$

In this approach, "$i-1$" refers to a positive peak while the successive "i" peak refers to a negative one, or vice versa [11, 33]. The terms "decay coefficients" refer to coefficients a, b, and c. Given below is the relationship between these coefficients and the damping coefficients:

$$2\alpha = a\frac{2}{\pi}\omega_{\phi}, \tag{11}$$

$$\beta = b\frac{3}{4}\frac{180}{\pi}, \tag{12}$$

$$\gamma = c\frac{8}{3\omega_{\phi}\pi}\left(\frac{180}{\pi}\right)^{2}. \tag{13}$$

2.2. DTMB 5512 model main particulars

The geometry of the DTMB 5512 is shown in Figure 2. Table 1 also provides information on the model where length (L), beam (B), draft (T), wetted surface area (S_W), block coefficient (C_B), longitudinal centre of gravity (LCG), vertical centre of gravity (VCG), roll radius of gyration (k_{ϕ}), natural roll period (T_{ϕ}). The metacentric height (GM), is defined as the distance between the centre of gravity (G) and the metacentre (M).

The first step in the research is to create a reliable nonlinear time-domain model capable of forecasting roll behavior while accounting for nonlinear factors. The experimental findings from Irvine et al. [34], Gökce and Kinaci [35] were used to validate the EKF approach used in this work. The hull was allowed to roll decay with an initial roll angle of $\phi_0 = 10^{\circ}$ and a forward velocity of $Fr = 0.41$. Figure 3 shows a simulation of a free-decay roll motion with a 15 *s* period and eighteen motion peaks. The fourth-order Runge-Kutta algorithm based on Eq. (4) was used to run the simulations for the time step $T_S = 0.001$ *s* (see Fig. 3). The target damping coefficients $\alpha = 0.3092$, $\beta = 0.8680$, $\gamma = -0.1524$ and $T_{\phi} = 1.54$ *s*, $\omega_{\phi} = 4.079$ *rad/s*. The simulation parameters are shown in Table 2. The rolling graph's peaks are listed in Table 3 for Figure 3. The correctness of the time step is illustrated by the roll extinction curves in Figure 4.

From the trend line equation, the coefficients α, β and γ were calculated. It can be seen that the R^2 value is extremely high indicating that predicted the values ϕ can represent the cubic model. Table 4 compares the both decay and extinction coefficients between the numerically estimated values and the target values, as well as the errors between them. There is a remarkable coincidence for the chosen time step ($T_S = 0.001$ *s*). For the numerical simulation, the maximum relative error is 0.99%, which is acceptable. It is evident that the suggested time step ($T_S = 0.001$ *s*) can be used to obtain the desired pseudo-experimental value. The variation of the equivalent damping coefficient (α_E) obtained from Eq. 3 is depicted in Figure

5. Upon examination of Figure 5, it is evident that the equivalent damping coefficient decreases over time and approaches a constant value. Furthermore, large heel angles result in high damping, and the damping coefficients show a substantial dependence on roll amplitude. This is due to the stronger vortex strengths at larger roll angles compared to smaller roll angles [13, 36].

This study examines the effect of measurement noise in the roll angle responses on the identification. The estimated response data from the simulated roll angle response time histories are then artificially corrupted by numerical noise.

2.3. Covariance matrix of measurement noise

The discrete measurement noise covariance characterizes the uncertainty in the pseudo-experiment simulations:

$$R_k = \sigma_m^2, \tag{14}$$

Where σ_m is the standard deviation. The simulated roll decaying motion is then corrupted with random Gaussian white noise, modeled with normally distributed white noise added to the calculated responses. To choose σ_m, several simulation runs were undertaken. The following are some of the values of σ_m that were tried in this work:

Scenario (a): Noise-free simulation $\sigma_{m1} = 1\text{x}10^{-4}$ *deg*.

Zero measurement noise in the EKF is acceptable theoretically for the noise-free simulation, however, this frequently leads to numerical problems [37]. To overcome this difficulty in noise-free simulations, standard deviations of the measurement errors are set as $\sigma_{m1} = 1\text{x}10^{-4}$ *deg.*

Scenario (b): $\sigma_{m2} = 0.1\text{x}10^{-1}$ *deg*.

The main idea of this case is to investigate the effects of the considered measurement noise contamination

Scenario (c): $\sigma_{m3} = 0.5\text{x}10^{-1}$ *deg*.

The final example aims to evaluate the effectiveness of method, particularly considering large signal noise contamination. Figure 6 displays the simulated noisy signals for a duration 15 *s* long.

When Figure 6 is examined, it becomes clear that the noisy measurement signal cannot be subjected to the ITTC-Recommended Procedure [1]. In this study, EKF is used to determine the equivalent roll damping coefficient and to remove noise from the output signal.

3. Extended Kalman Filter

The filtering strategy transforms the parameter estimation problem into a state estimation problem, which is an indirect method for parameter estimation. To achieve this, the system state vector is intentionally extended to include the unknown parameters as additional state variables. In this study, EKF was used to estimate parameters α_E and ω_ϕ given in Eq. (6). By incorporating unknown parameters to the state space vector, the equations for parameter estimation and state update become non-linear. Consequently, the EKF technique enables the simultaneous estimation of parameters and states. A detailed explanation of the Kalman filter theory can be found in Gelb [38] and Zarchan [39]. This section will only provide a summary. An example of a general non-linear system is:

$$\dot{x} = f(x, u) + w, \tag{15}$$

where x is a vector of system states, u is a vector of inputs, f is a nonlinear operator and w is a random zero-mean process noise. The process-noise matrix is provided by:

$$Q = E(ww^T), \tag{16}$$

Where $E(ww^T)$ is the expected value of (ww_T). The measurement equation is considered a nonlinear function of the states according to:

$$z = h(x) + v, \tag{17}$$

Where v is the observation noise and h is the observation function. The measurement noise matrix is described as follows:

$$R = E(vv^T), \tag{18}$$

where $E(vv^T)$ is the expected value of (vv^T). Measurements are nonlinear and discrete can be represented by the following equations:

$$z_k = h(x_k) + v_k, \tag{19}$$

and

$$R_k = E(v_k v_k^T). \tag{20}$$

The following Jacobians are used to define the systems dynamics matrix (F) and measurement matrices (H).

$$F \approx \left.\frac{\partial f(x)}{\partial x}\right|_{x=\hat{x}}, \tag{21}$$

$$H \approx \left.\frac{\partial h(x)}{\partial x}\right|_{x=\hat{x}}. \tag{22}$$

Unknown parameters are added to the state dynamic matrix in this investigation. This is the form of the augmented state vector for the free decay motion:

$$\dot{x} = \begin{bmatrix} x_1 & x_2 & x_3 & x_4 \end{bmatrix}^T, \tag{23}$$

where,

$$x_1 = \phi,\ x_2 = \dot{\phi},\ x_3 = \alpha_E,\ x_4 = \omega_\phi^2, \tag{24}$$

the system's dynamical equation is rewritten in state-space form as follows:

$$\dot{x} = f(x_1, x_2, x_3, x_4), \tag{25}$$

Where f is a nonlinear function. The Taylor-series expansion for e^{FT_S} can approach the fundamental matrix Φ_k:

$$\Phi_k = I + FT_S + \frac{F^2T_S^2}{2!} + \frac{F^3T_S^3}{3!} + ... \tag{26}$$

The identity matrix is called I, T_S represents for sampling time and F is the systems dynamics matrix. The Kalman gains K_k are calculated from the matrix Riccati equations while the filter is running. The following definition applies to the Riccati equations, a set of iterative matrix equations:

$$\begin{aligned} M_k &= \Phi_k P_{k-1} \Phi_k + Q_k, \\ K_k &= M_k H^T \left(H M_k H^T + R_k\right)^{-1}, \\ P_k &= \left(I - K_k H\right) M_k. \end{aligned} \tag{27}$$

P_k is a covariance matrix that shows errors in state estimates following an update, and M_k is a covariance matrix that shows errors in state estimates prior to an update. By using the continuous process-noise matrix, Q, the discrete process-noise matrix, Q_k, can be derived as defined:

$$Q_k = \int_0^{T_S} \Phi(\tau) Q \Phi^T(\tau)\, dt. \tag{28}$$

With EKF estimation of the state vector is given as:

$$\hat{x}_k = \bar{x}_k + K_k \left[z_k - h\left(\bar{x}_k\right)\right]. \tag{29}$$

To predict the state vector, we integrated the nonlinear differential equations using the Runge-Kutta method.

$$\bar{x}_k = \hat{x}_{k-1} + \dot{\hat{x}}_{k-1} T_S, \tag{30}$$

here the derivative is obtained from Eq. (31), [37]:

$$\dot{\hat{x}}_{k-1} = f\left(\hat{x}_{k-1}\right). \tag{31}$$

In the above EKF, the values of the new state $\hat{x}_k$ are estimated iteratively. In-house code, written in the FORTRAN programming language, was used to solve the four-state EKF equations and the Riccati equations.

4. Estimation of the equivalent damping coefficient and natural frequency via augmented extended Kalman filtering

An evaluation of the EKF's capability for equivalent roll damping coefficient estimation in a nonlinear state-space model of freely decaying motion was attempted. The first phase in the filtering process involves estimating the initial values of the state variables.

4.1. Initial estimation error

Theoretical values for the errors in the estimation of the first, second, third, and fourth states are denoted by P_{11}, P_{22} , P_{33}, and P_{44}, respectively. Due to the assumption that we lack any a priori knowledge of the natural frequency and equivalent-damping coefficient. The initial covariance matrix's diagonal values are infinite ($P_{33} = P_{44} = \infty$) and the filter state of the square of natural frequency $\hat{x}_{40}$ and equivalent damping coefficient$\hat{x}_{30}$ are initialized to zero ($\hat{x}_{30} = \hat{x}_{40} = 0$). These errors can be seen in the initial covariance matrix. The original covariance matrix's diagonal elements must not be zero, even when the roll angle x_{10} and roll angular velocity x_{20} first filter estimations are close to the right values.

The filter fails the test because the initial values are assumed to be true, and the initial error covariance is set to zero [39]. Consequently, small values were chosen for the error covariance matrices of the roll angle and angular velocity:

$$H = \begin{bmatrix} 1 & 0 & 0 & 0 \end{bmatrix}, \tag{32}$$

$$\hat{x}_0 = \begin{bmatrix} \phi_{10} & 0 & 0 & 0 \end{bmatrix}^T, \tag{33}$$

$$P_0 = \mathrm{diag}\begin{pmatrix} 0.1 & 0.1 & \infty & \infty \end{pmatrix}. \tag{34}$$

4.2 Model Error

The process-noise covariance matrix Q_k should be zero or small if the real-world Kalman filter model is regarded to be accurate. Large values of Q_k show that we really mistrust the accuracy of the Kalman filter to model the real world. The EKF model assumes α_E is a constant by utilizing zero process noise [39]. The performance of EKF is mainly controlled using the process noise covariance matrix. Therefore, to increase the robustness of the final filter, process noise can be added the derivative of the α_E. For the non-linear model used in this study, it can be assumed that the continuous process-noise matrix is [39].

$$Q = \mathrm{diag}\begin{pmatrix} 0 & 0 & \sigma_P^2 & 0 \end{pmatrix}. \tag{35}$$

According to Eq. 28, the discrete process-noise matrix (Q_k) can be generated using the continuous process-noise matrix. Standard deviations of the process noise (σ_p) can be used as an adjusting parameter to enhance the filter's overall performance because they effectively increase or decrease noise in the high-ordered term.

As a result, the accuracy of the Kalman filtering method is directly influenced by the process noise covariance matrix [39]. Various Q_k values were employed to explore their impact on the precision of the estimator.

To determine whether the EKF was operating correctly, we compared the estimations obtained by the EKF to the ITTC–Recommended Procedures and Guidelines [1] in all the work we have completed thus far. It is impossible to know the actual system states during real filter operation. A comparison between the measured residual and the theoretical estimate is necessary to assess if the filter is operating correctly. A more detailed explanation can be found in Ozdemir [13].

A number of simulation runs were performed to select σ_p, and the following are some of the values of σ_p^2 that were tried in this work:

$$\begin{aligned} \sigma_{p1}^2 &= 1\times10^{-5}, \\ \sigma_{p2}^2 &= 1\times10^{-4}, \\ \sigma_{p3}^2 &= 1\times10^{-3}. \end{aligned} \tag{36}$$

5. Results

Simulations were performed for 15000 equally spaced time points ($T_s = 0.001$ *s*) with a measurement sampling rate of 1000 *Hz*. This section demonstrates a simulation that illustrates how the EKF's processing of noisy roll angle measurements can be utilized to estimate the roll angle (ϕ), natural frequency (ω_ϕ), and equivalent damping coefficient (α_E). When different values of σ_p are employed in the EKF, the true state and the estimated first state are shown in Figures 7-9. The estimation of the roll angle is found to be a good match for the simulation result. These results demonstrate the outstanding estimation quality of the filter since the estimated roll angle looks to be almost identical. Furthermore, the measurement noise was well filtered by the EKF. It is worth noting that the larger the process noise, the smaller the prediction error, which is an expected result [37].

The same conclusion can be seen from the root mean square error (RMSE) values, which are given in Table 5. RMSE was used as an indicator to measure the performance of the Kalman filter. It measures the degree of discrepancy between two sets of data. The RMSE is calculated by:

$$\mathrm{RMSE} = \sqrt{\frac{\sum_{k=1}^{N}\left(\hat{x}_k - z_k\right)^2}{N}}, \tag{37}$$

Where $\hat{x}_k$ is the state estimate from the filter, z_k is the calculated value from pseudo-experimental values and N is the number of measurements. From the data in the table, it can be seen that the EKF filters appeared to be working after the addition of process noise (i.e., σ_{p3}). Examining the error in the estimates (i.e., the difference between actual signal and estimate) a performance indicator is necessary.

To verify the proper functioning of the filter, Figure 10 compares the inaccuracy in the estimate of the roll angle $\phi(x_1)$, of the EKF with the theoretical values derived from the covariance matrix (i.e., square root of P_{11} for the first state, square root of P_{22} for the second state, etc.). The simulated error in the estimation of roll angle outside the theoretical error limitations was obtained using the Riccati equations covariance matrix when the process noise was small (i.e., σ_{p1}), showing that the filter is not functioning properly.

Figure 10 now demonstrates that the filter appears to be operating because of errors in the estimations of roll angle within the theoretical c restrictions after the high process noise was added to the Kalman filter (i.e., σ_{p3}). It was demonstrated in Figure 10 that the error and theoretical bounds can be used to determine whether or not the filter is performing properly.

Figure 11 displays the time histories of the estimated equivalent damping coefficient (α_E) for scenarios (a), (b), and (c), along with the true state. Due to an incorrect filter setup, a significant transient is observed at the beginning, but it quickly converges to the true parameters. As the covariance decreases, as depicted in Figure 10, the oscillation value of the convergence curve in Figure 11 also diminishes, ultimately leading the parameter to converge to its true value. This shows that the EKF algorithm accurately estimates the states of free-decay roll motion for noise-free simulation. As can be seen, the estimated parameters exhibit more severe oscillations in the recursive process over time due to significant noise interference. It can be seen from Figure 11 that incorporating process noise could somewhat enhance the estimates. The estimations obtained using EKF are highly reliant on the σ_p, as evident in the same figure. The equivalent linear damping coefficient estimates of the Kalman filter align more closely with the exact results when process noise is introduced. The parameter estimates are more delayed as σ_p decreases, and they sometimes differ dramatically from the exact values. However, the inclusion of process noise comes with a cost. As observed in Figure 11, estimates made with large process noise are noisier compared to those made with small process noise. It is found that the EKF can estimate accurate states when there is noise and this can be easily explained by using Figure 12. The filter is able to pay greater attention to the measurements because of the larger Kalman gains [39].

Examining the residuals, or the discrepancy between the measured values and the estimates, is one technique to assess the accuracy of the observer. White noise with a mean of zero should make up the residuals for an accurate observer. This is further supported by the examination of measurement residuals that roughly resemble zero mean white noise. Figure 13 shows that the mean of the residuals for σ_{p3} is certainly close to zero and the standard deviation's closest value is represented by the following [39]:

$$\sigma_{\text{APPROX}} \approx \frac{\text{Peak to Peak}}{6}, \tag{38}$$

which represents the actual value in theory.

Since the natural frequency is constant, model error is not included in its derivative. As depicted in Figure 14, the variation in the natural frequency estimates of the filter is very small due to the model error involved in the damping coefficient. The simulation resulted in a natural frequency of $\omega_\phi = 4.080$ *rad/s*, deviating by only 0.02% from the actual value of $\omega_\phi = 4.079$ *rad/s*.

In Figure 15, the variation of the linear equivalent-damping coefficient estimated by EKF with time is shown as a result of modeling with different sampling times. All other filter parameters remain the same with the ideal case $T_S = 0.001s$. It can be seen from Figure 15 that as the measurement noise increases, the error value increases in the solutions carried out at large sampling periods. The effect of sampling time on the results is reduced when there is small measurement noise.

Figure 16 shows the natural frequency calculated for three different scenarios at a sampling period of $T_S = 0.01s$. The simulations calculated a natural frequency of $\omega_\phi = 4.086$ *rad/s*, which differs by 0.17% from the actual value ($\omega_\phi = 4.079$ *rad/s*). From this figure, it has been seen that the sampling time has no significant effect on the estimation of the natural frequency.

6. Contribution of this study

In this study, both α_E and ω_ϕ, as defined in Eq. (6), are simultaneously estimated using the EKF method. The parameter identification method presented in this paper can calculate the time-varying linear equivalent-damping coefficient from freely rolling decay motion. The proposed technique can effectively eliminate noise from the measurement signals. Moreover, it was suggested to apply an alternate and practical tool for system identification and state estimate. Of particular note, the proposed parameter estimation method can also be applied to motions with high degrees of freedom.

The suggested method is still fairly robust even if any measurement noise is incorporated in the provided additional information on measured data. When the DTMB 5512 research hull's hydrodynamic parameters were estimated using an EKF, there was not much of a difference between the predicted values and exact values of the parameters. The key reason for this is a precise estimating model. Moreover, with the EKF method, time-varying parameter estimation was made without the need for curve fitting and knowing the natural frequency. This result is an important advantage of EKF over the method proposed by the ITTC [1]. As an alternative to the procedure proposed by the ITTC–Recommended Procedures and Guidelines [1], a method is presented to determine the time-varying equivalent-damping coefficient.

These examples demonstrate that, even though the parameters were considered as the systems' states, implying potential changes over time, they can still converge to stable values. This approach allows for the estimation of linear equivalent damping coefficient and natural

frequency without requiring prior knowledge of the input. The study reveals that the initial covariance matrix has little effect on the EKF's performance. Furthermore, the EKF algorithm demonstrates compatibility between the estimated roll angle response and the actual roll angle response, despite the chaotic nature of the measurement signal caused by noise. The EKF algorithm effectively filters out measurement noise, while its accuracy is impacted by measurement noise in Kalman filter-based inversion. Interestingly, measurement noise has no discernible impact on estimating natural frequencies. It can be concluded that both process noise and sampling time do not affect natural frequency estimation. Keeping process noise high and the sampling period low allows for the estimation of a linear equivalent damping coefficient in the presence of high measurement noise.

7. Conclusion

In this study, a novel method for determining the equivalent linear roll damping coefficient and natural frequency was presented based on the augmented EKF. The EKF method is accurate in determining both time-varying linear equivalent damping coefficient and natural frequency. It may be concluded that the proposed method can evaluate time-varying damping coefficient and natural frequency with sufficient accuracy and can be used as a design tool for ship design. Future research work will focus on the extension of the proposed method. Currently, the recommended method considers free roll decay motion only. The method introduced in this article will be applied to experimental data in the future. Additionally, there is potential for applying the method to high-degree-of-freedom motions. It is planned to examine the 2DOF heave and pitch motion, which are among the most common motions in ships.

Disclosure statement

The author reported no potential conflict of interest.

Funding

The author received no financial support for the research, authorship, and/or publication of this article.

Nomenclature

B	Beam	VCG	Vertical position of centre of gravity
C_B	Block coefficient	v_k	Vector of measurement error
F_k	Systems dynamics matrix	w_k	Vector of disturbances (errors in the system)
GM	Transversal metacentric height	$\hat{x}_k$	Vector of estimated value of states variables
H_k	Measurement matrix	z_k	Vector of measurements
K_k	Kalman gain matrix	ϕ	Roll angle
k_ϕ	Roll radius of gyration	ϕ_m	Mean roll angle
L	Length	ϕ_i	Roll angle amplitude
LCG	Longitudinal position of the centre of gravity	Φ_k	Transition or system matrix of discrete system
S_W	Wetted surface area	ω	Damped frequency
P_k	Covariance matrix of estimate error	ω_ϕ	Natural frequency
Q_k	Covariance matrix of system noise	α	Linear extinction coefficient
R_k	Covariance matrix of measurement noise	α_E	Equivalent linear extinction coefficient
T	Draft	β	Quadratic extinction coefficient
T_S	Sampling time	γ	Cubic extinction coefficient
T_ϕ	Natural roll period	σ	Standard deviation

REFERENCES

1. ITTC "Numerical Estimation of Roll Damping. Recommended Procedures", 33 (2011).
2. Begovic, E., Day, A. H., and Incecik, A. "An experimental study of hull girder loads on an intact and damaged naval ship. Ocean Engineering", 133, pp. 47–65 (2017). DOI: 10.1016/j.oceaneng.2017.02.001
3. Igbadumhe, J. F., Sallam, O., Fürth, M., et al. "Experimental Determination of Non-Linear Roll Damping of an FPSO Pure Roll Coupled with Liquid Sloshing in Two-Row Tanks", Journal of Marine Science and Engineering, 8(8), (2020). DOI: 10.3390/JMSE8080582
4. Ikeda, Y., Himeno, Y., and Tanaka, N. "On eddy making component of roll damping force on naked hull", J. Soc. Nav. Archit. Jpn., 142, pp. 59–69 (1977).
5. Froude, W. "On Resistance in Rolling of Ships", Naval Science, III, 107 (1874).
6. Himeno, Y. "Prediction of Ship Roll Damping - State of the Art" University of Michigan Department of Naval Architecture and Marine Engineering, (Report), (239) (1981).
7. Spouge, J. "Non-linear analysis of large-amplitude rolling experiments", Int. Shipbuild. Prog, 35, pp. 271–324 (1988).
8. Wassermann, S., Feder, D. F., and Abdel-Maksoud, M. "Estimation of ship roll damping - A comparison of the decay and the harmonic excited roll motion technique for a post panamax container ship", Ocean Engineering, 120, pp. 371–382 (2016). DOI: 10.1016/j.oceaneng.2016.02.009
9. Yu, L., Ma, N., and Wang, S. "Parametric roll prediction of the KCS containership in head waves with emphasis on the roll damping and nonlinear restoring moment", Ocean Engineering, 188 (2019). DOI: 10.1016/j.oceaneng.2019.106298
10. Manderbacka, T., Themelis, N., Bačkalov, I., et al. "An overview of the current research on stability of ships and ocean vehicles: The STAB2018 perspective", Ocean Engineering, 186, (2019). DOI: 10.1016/j.oceaneng.2019.05.072
11. Rodríguez, C. A., Ramos, I. S., Esperança, P. T. T., et al. "Realistic estimation of roll damping coefficients in waves based on model tests and numerical simulations", Ocean Engineering, 213, 107664, (2020). DOI: 10.1016/j.oceaneng.2020.107664
12. Sun, J., James Hu, S. L., and Li, H. "Nonlinear roll damping parameter identification using

free-decay data", Ocean Engineering, 219(December 2020), 108425, (2021). DOI: 10.1016/j.oceaneng.2020.108425

13. Ozdemir, Y. H. "Estimation of ship roll damping and natural frequency using an extended Kalman filter applied to URANS output", Sadhana - Academy Proceedings in Engineering Sciences, 48(3), (2023). DOI: 10.1007/s12046-023-02232-x
14. Hashimoto, H., Omura, T., Matsuda, A., et al. "Several remarks on EFD and CFD for ship roll decay", Ocean Engineering, 186, 106082 (2019). DOI: 10.1016/j.oceaneng.2019.05.064
15. Jiang, Y., Ding, Y., Sun, Y., et al. "Influence of bilge-keel configuration on ship roll damping and roll response in waves", Ocean Engineering, 216(2), 107539, (2020). DOI: 10.1016/j.oceaneng.2020.107539
16. Bekhit, A., and Popescu, F. "Uranse-based numerical prediction for the free roll decay of the dtmb ship model", Journal of Marine Science and Engineering, 9(5), (2021). DOI: 10.3390/jmse9050452
17. Kalman, R. E., and Bucy, R. S. "New results in linear filtering and prediction theory", Journal of Fluids Engineering, Transactions of the ASME, 83(1), pp. 95–108 (1961). DOI: 10.1115/1.3658902
18. Welch, G., and Bishop, G. "Technical report, Proceedings of SIGGRAPH" Course 8, (2001).
19. Reina, G., Leanza, A., and Messina, A. "Terrain estimation via vehicle vibration measurement and cubature Kalman filtering", JVC/Journal of Vibration and Control, 26(11–12), pp. 885–898 (2020). DOI: 10.1177/1077546319890011
20. Chowdhary, G., and Jategaonkar, R. "Aerodynamic parameter estimation from flight data applying extended and unscented Kalman filter", Aerospace Science and Technology, 14(2), pp. 106–117 (2010). DOI: 10.1016/j.ast.2009.10.003
21. Megyesi, D., Bréda, R., and Schrötter, M. "Adaptive control and estimation of the condition of a small unmanned aircraft using a Kalman filter", Energies, 14(8), (2021). DOI: 10.3390/en14082292
22. Wang, Q., Zheng, F., Qian, W., et al. "A practical filter error method for aerodynamic parameter estimation of aircraft in turbulence", Chinese Journal of Aeronautics, 36(2), (2023). DOI: 10.1016/j.cja.2022.05.008
23. Wang, Z., Dong, M., Qin, Y., et al. "Suspension system state estimation using adaptive Kalman filtering based on road classification", Vehicle System Dynamics, 55(3), pp. 371–398 (2017). DOI: 10.1080/00423114.2016.1267374
24. Zhi, L., Yu, P., Li, Q. S., et al. "Identification of wind loads on super-tall buildings by Kalman filter", Computers and Structures, 208, pp. 105–117 (2018). DOI: 10.1016/j.compstruc.2018.07.002
25. Wu, Y., and Chen, X. "Identification of nonlinear aerodynamic damping from stochastic crosswind response of tall buildings using unscented Kalman filter technique", Engineering

Structures, 220, 110791, (2020). DOI: 10.1016/j.engstruct.2020.110791

26. Yang, B., Zhu, H., Zhang, Q., et al. "Identification of wind loads on a 600 m high skyscraper by Kalman filter", Journal of Building Engineering, **63**(PA), 105440, (2023). DOI: 10.1016/j.jobe.2022.105440
27. Song, M., Astroza, R., Ebrahimian, H., et al. "Adaptive Kalman filters for nonlinear finite element model updating", Mechanical Systems and Signal Processing, 143, 106837, (2020). DOI: 10.1016/j.ymssp.2020.106837
28. Fauriat, W., Mattrand, C., Gayton, N., et al. "Estimation of road profile variability from measured vehicle responses", Vehicle System Dynamics, 54(5), pp. 585–605 (2016). DOI: 10.1080/00423114.2016.1145243
29. Reina, G., and Messina, A. "Vehicle dynamics estimation via augmented Extended Kalman Filtering. Measurement", Journal of the International Measurement Confederation, 133, pp. 383–395 (2019). DOI: 10.1016/j.measurement.2018.10.030
30. Liu, Y. J., Dou, C. H., Shen, F., et al. "Vehicle State Estimation Based on Unscented Kalman Filtering and a Genetic-particle Swarm Algorithm", Journal of The Institution of Engineers (India): Series C, 102(2), pp. 447–469 (2021). DOI: 10.1007/s40032-021-00663-1
31. Rodríguez, A. J., Sanjurjo, E., Pastorino, R., et al. "State, parameter and input observers based on multibody models and Kalman filters for vehicle dynamics", Mechanical Systems and Signal Processing, 155, (2021). DOI: 10.1016/j.ymssp.2020.107544
32. Xu, W., Yang, J., Wei, H., et al. "Error-state Kalman filter-based localization algorithm with velocity estimation for deep-sea mining vehicle", Ocean Engineering, 264, (2022). DOI: 10.1016/j.oceaneng.2022.112331
33. Begovic, E., and Bertorello, C. "Omae2013-10620 Roll Damping Coefficients Assessment and Comparison for. Omae", pp. 1–9 (2013).
34. Irvine, M., Longo, J., and Stern, F. "Forward speed calm water roll decay for surface combatant 5415: Global and local flow measurements", Transactions - Society of Naval Architects and Marine Engineers, 121(4), pp. 549–566 (2015). DOI: 10.5957/jsr.2013.57.4.202
35. Gokce, M. K., and Kinaci, O. K. "Numerical simulations of free roll decay of DTMB 5415", Ocean Engineering, 159, pp. 539–551 (2018). DOI: 10.1016/j.oceaneng.2017.12.067
36. Irkal, M. A. R., Nallayarasu, S., and Bhattacharyya, S. K. "Numerical prediction of roll damping of ships with and without bilge keel", Ocean Engineering, 179(March), pp. 226–245 (2019). DOI: 10.1016/j.oceaneng.2019.03.027
37. Simon, D. "Optimal state estimation: Kalman, H∞, and nonlinear approaches. Optimal State Estimation: Kalman, H∞, and Nonlinear Approaches", (2006). DOI: 10.1002/0470045345
38. Gelb, A. "Applied optimal estimation. Proceedings of the IEEE", (Vol. 64), (2001).
39. Zarchan, B. P. "Fundamentals of Kalman Filtering : A Practical Approach" (Progress in Astronautics and Aeronautics)", (2011).

List of Captions

Figure captions

Table captions

Table 1. Hydrostatic properties of the DTMB hull model 5512

Table 2. Simulation parameters

Table 3. The numerical peaks of the roll response

Table 4. Comparison of the decay and extinction coefficients

Table 5. RMSE values for the first state for various choices of σ_{p3} in EKF(s)

Figures

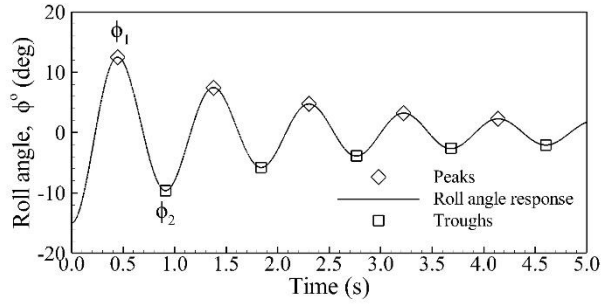

Figure 1. Typical roll decay curve

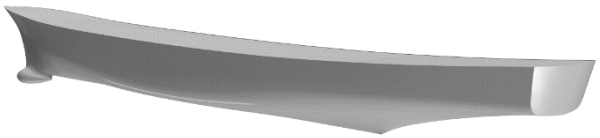

Figure 2**.** The DTMB model 5512 seen from a perspective

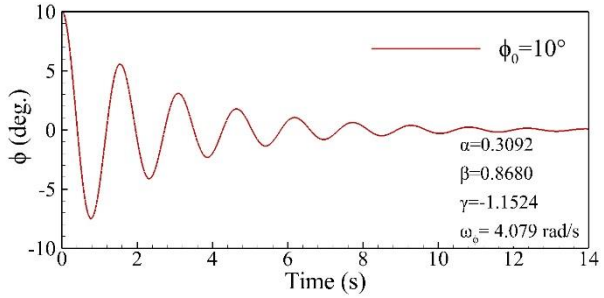

Figure 3. Simulated free roll decay with an initial angle $\phi_0 = 10^\circ$ at $\mathrm{Fr} = 0.417$ by running the fourth-order Runge-Kutta algorithm ($T_S = 0.001 s$)

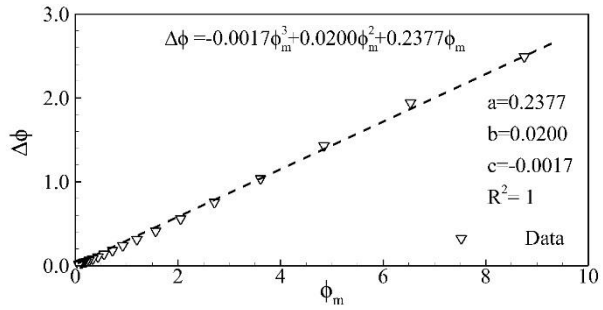

Figure 4. Extinction curve ($T_S = 0.001s$)

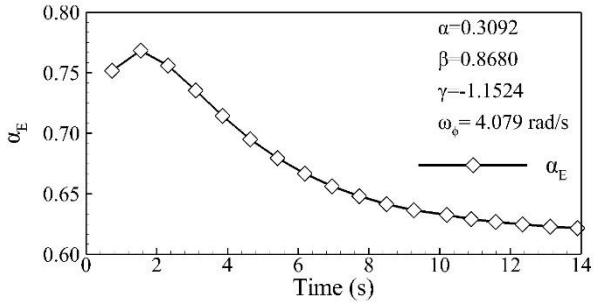

Figure 5. Equivalent linear damping coefficient ($T_S = 0.001s$)

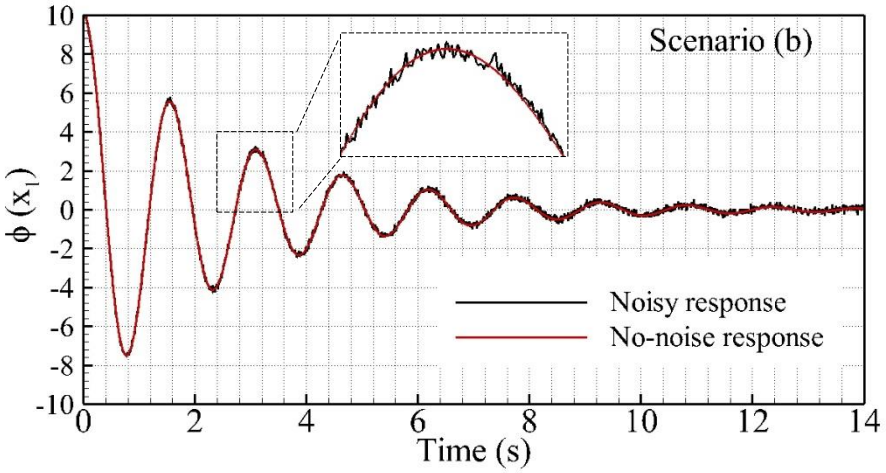

(a)

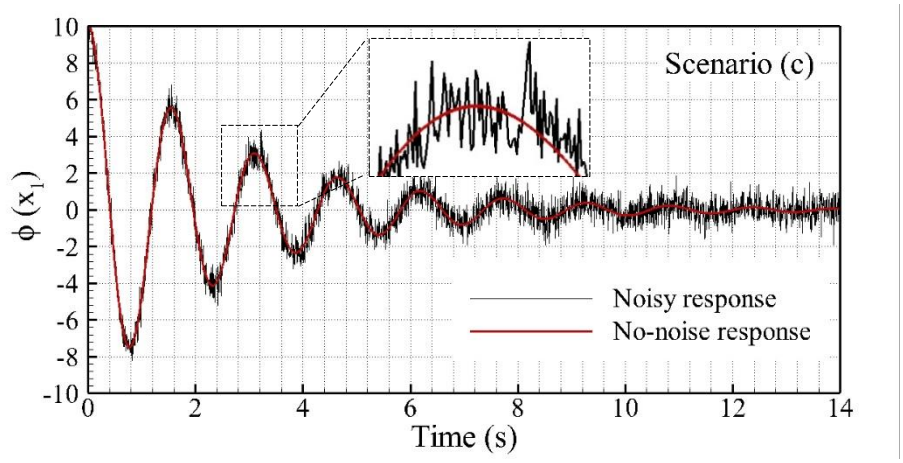

(b)

Figure 6. The simulated noisy signals ($T_S = 0.001\,s$): (a) $\sigma_{m2} = 1\text{x}10^{-2}\,deg$;

(b) $\sigma_{m3} = 0.5\text{x}10^{-1}\,deg$

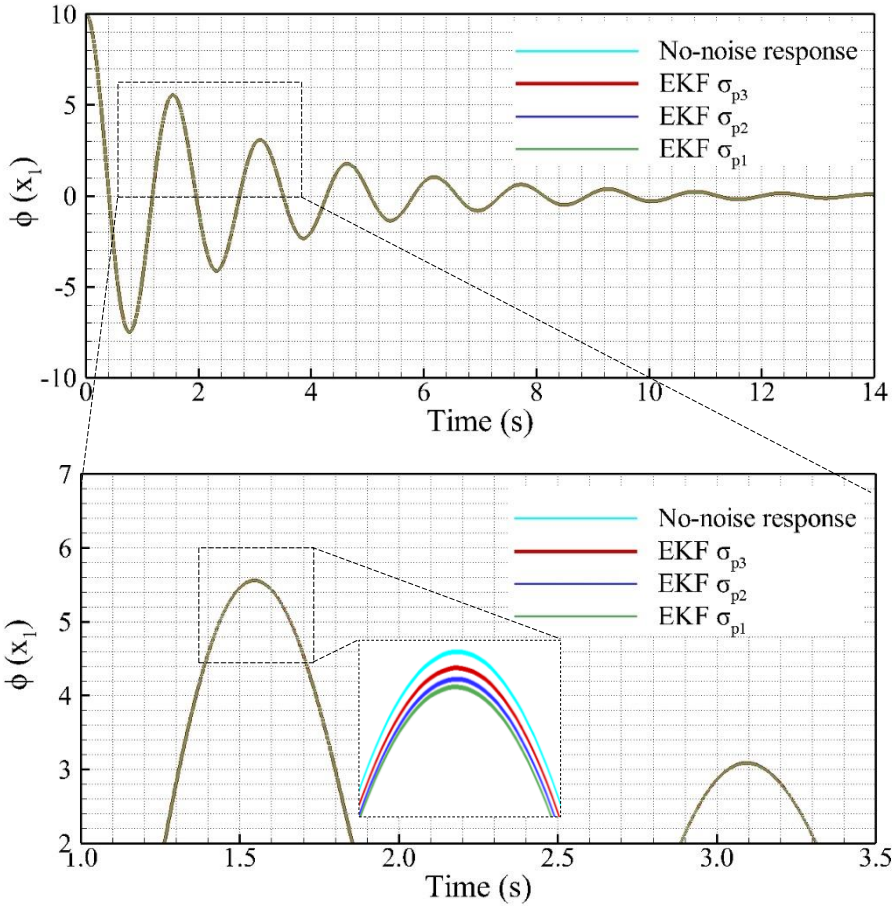

Figure 7. Comparison of actual and estimated roll angle for Scenario (a) (noiseless input)

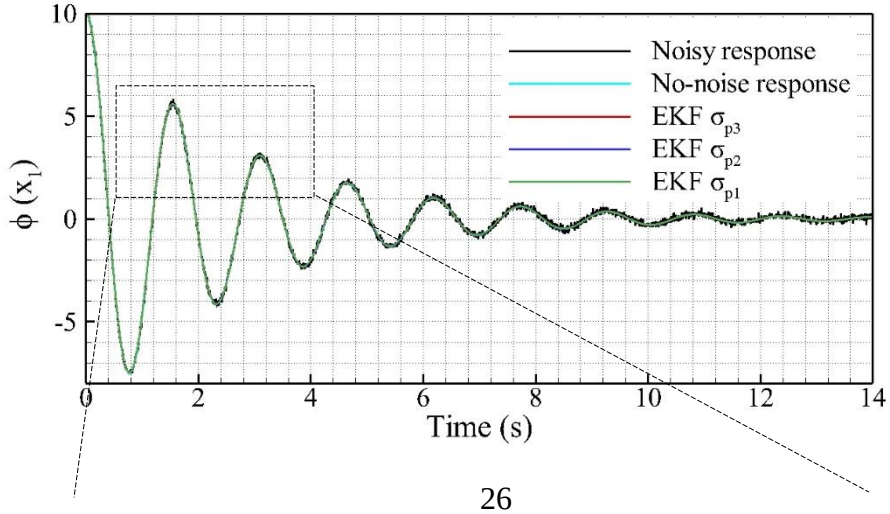

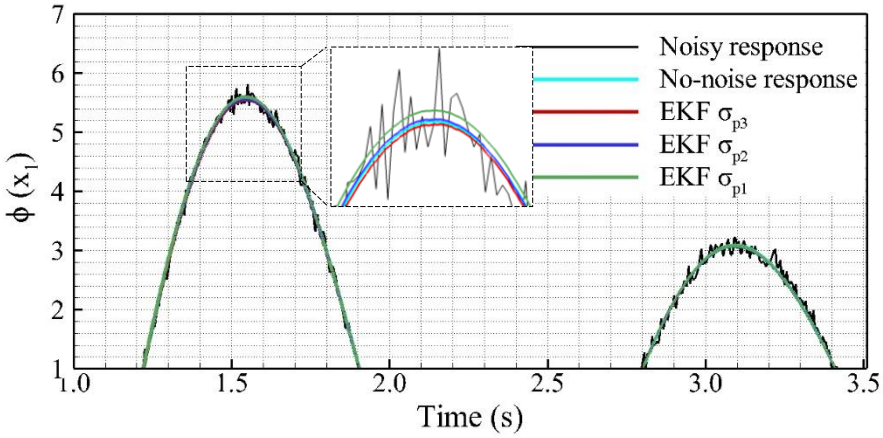

Figure 8. Comparison of actual and estimated roll angle for scenario (b)

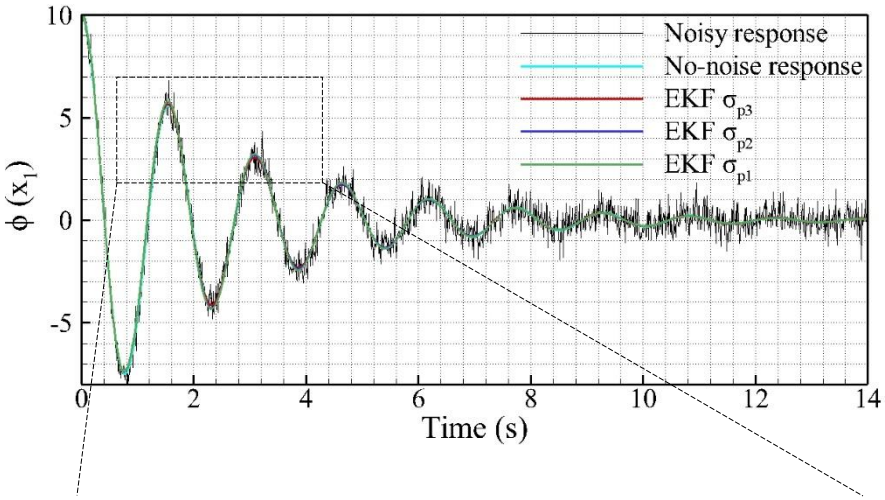

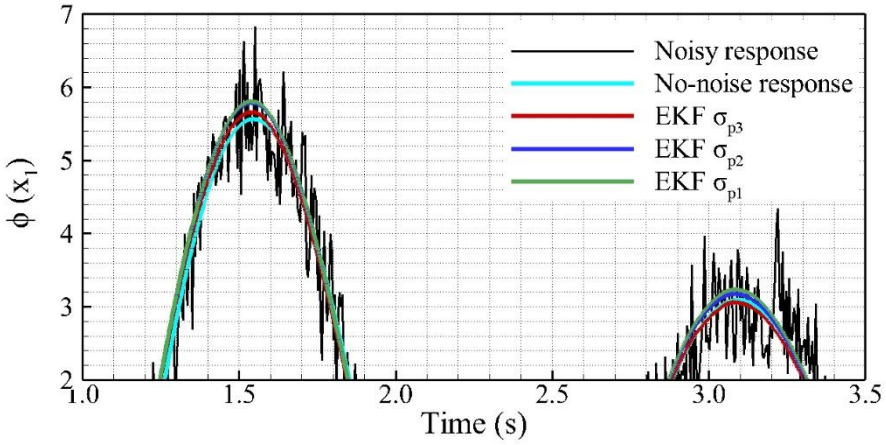

Figure 9. Comparison of actual and estimated roll angle for scenario (c)

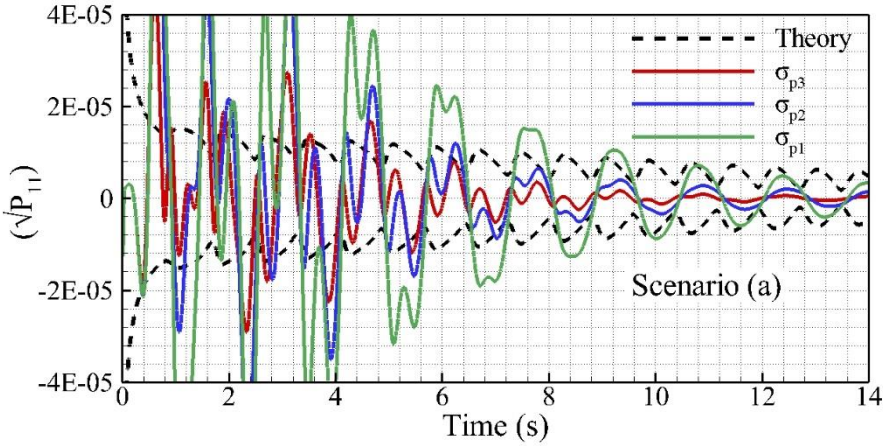

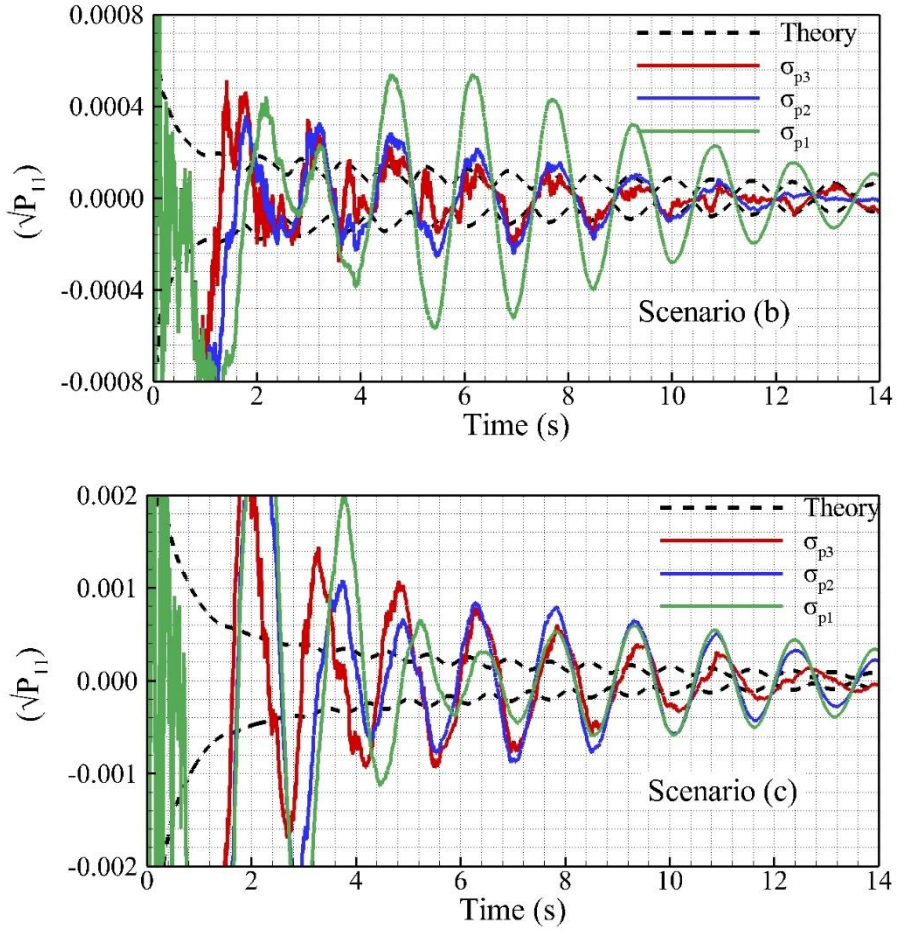

Figure 10. Covariance propagation of the $\phi(x_1)$ for three simulation scenarios

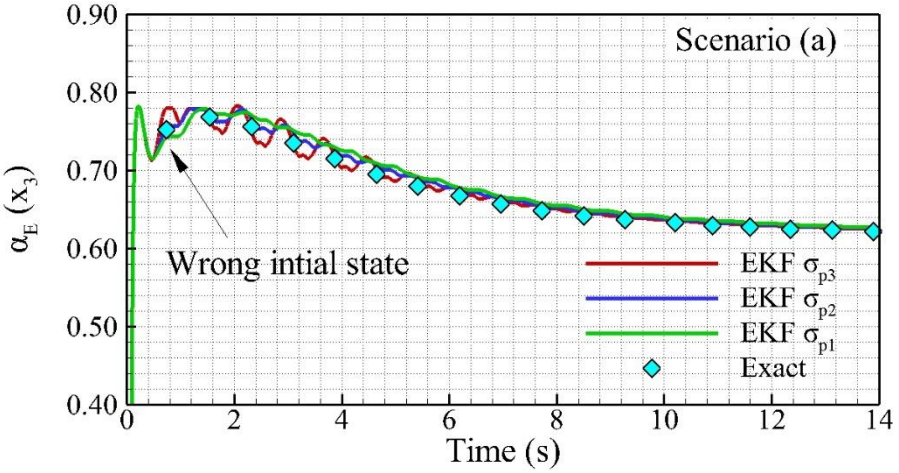

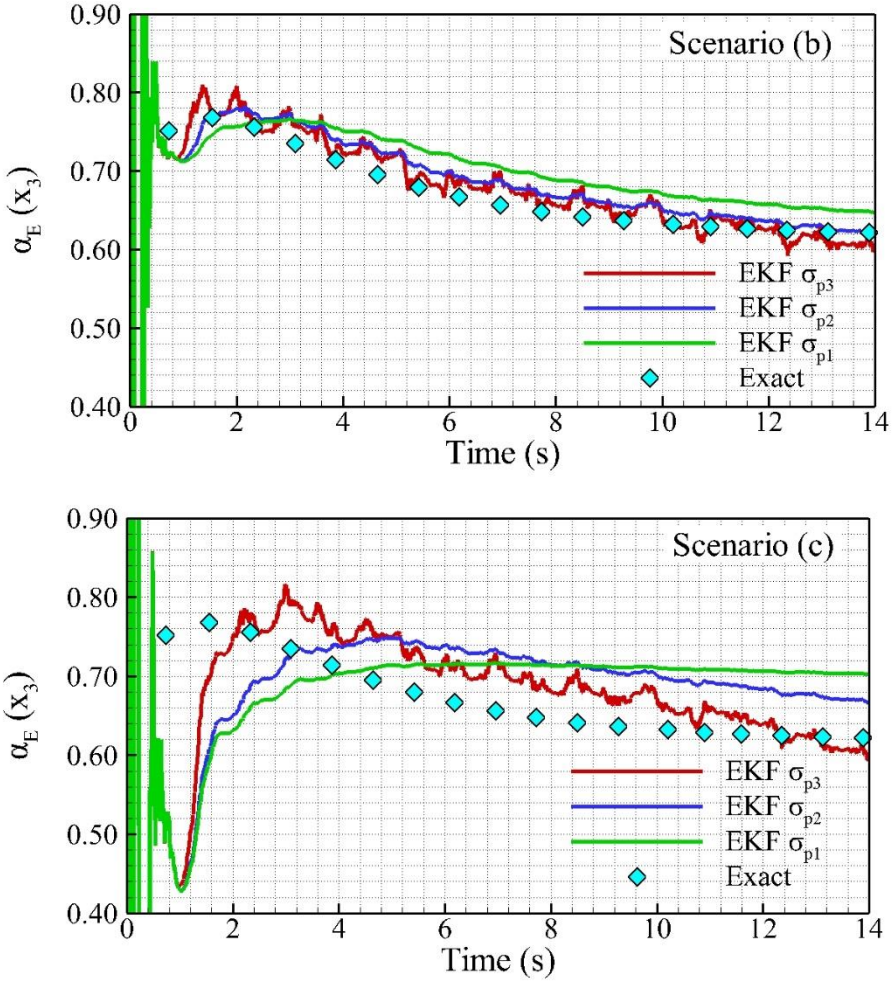

Figure 11. The estimated value of equivalent linear damping coefficient (α_E) for three scenarios

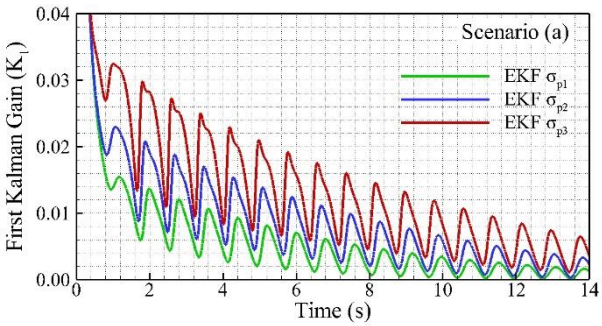

Figure 12. The effects of process noise covariance matrix Q on the Kalman Gain

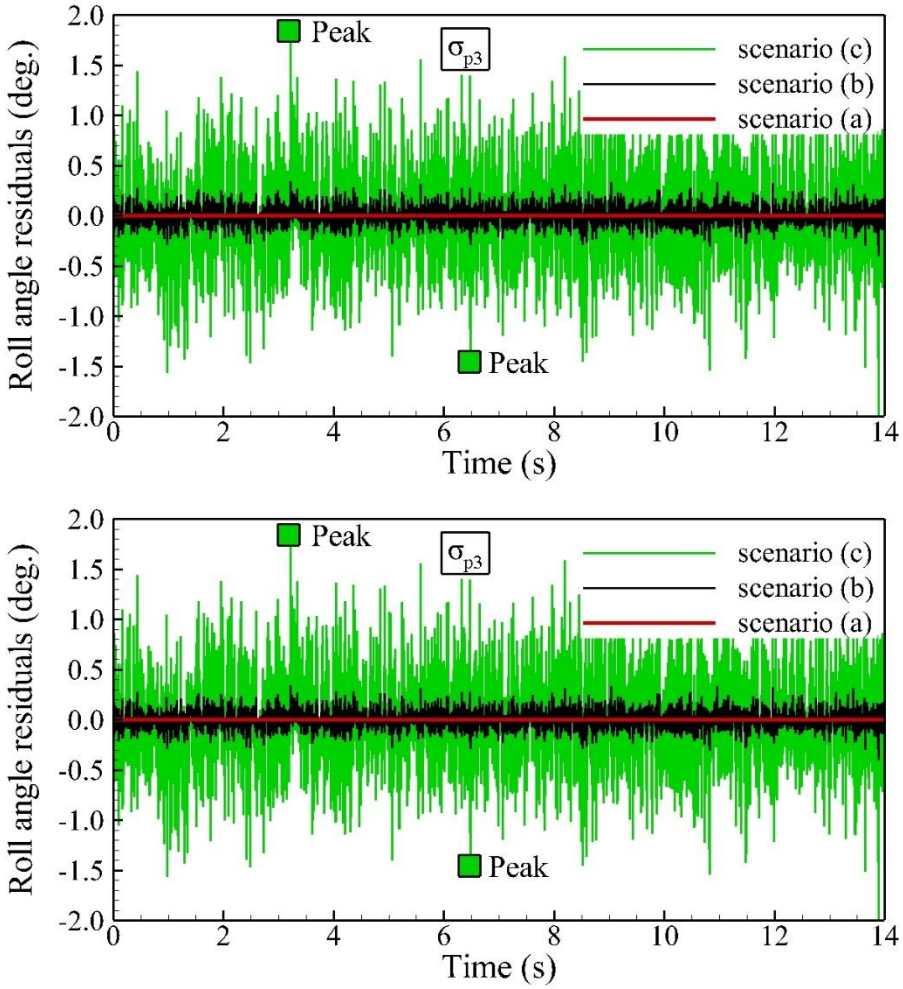

Figure 13. Residuals from EKF(s)

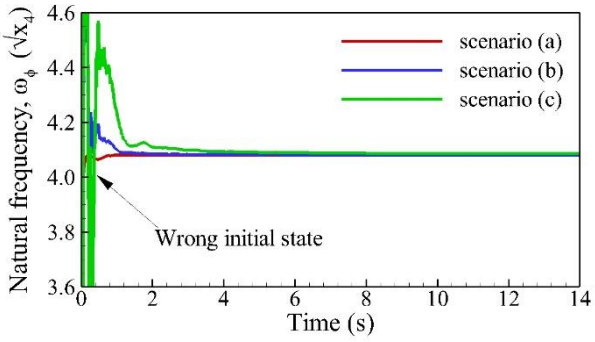

Figure 14. The estimated value of natural frequency (ω_ϕ) for the various sets of the process noise

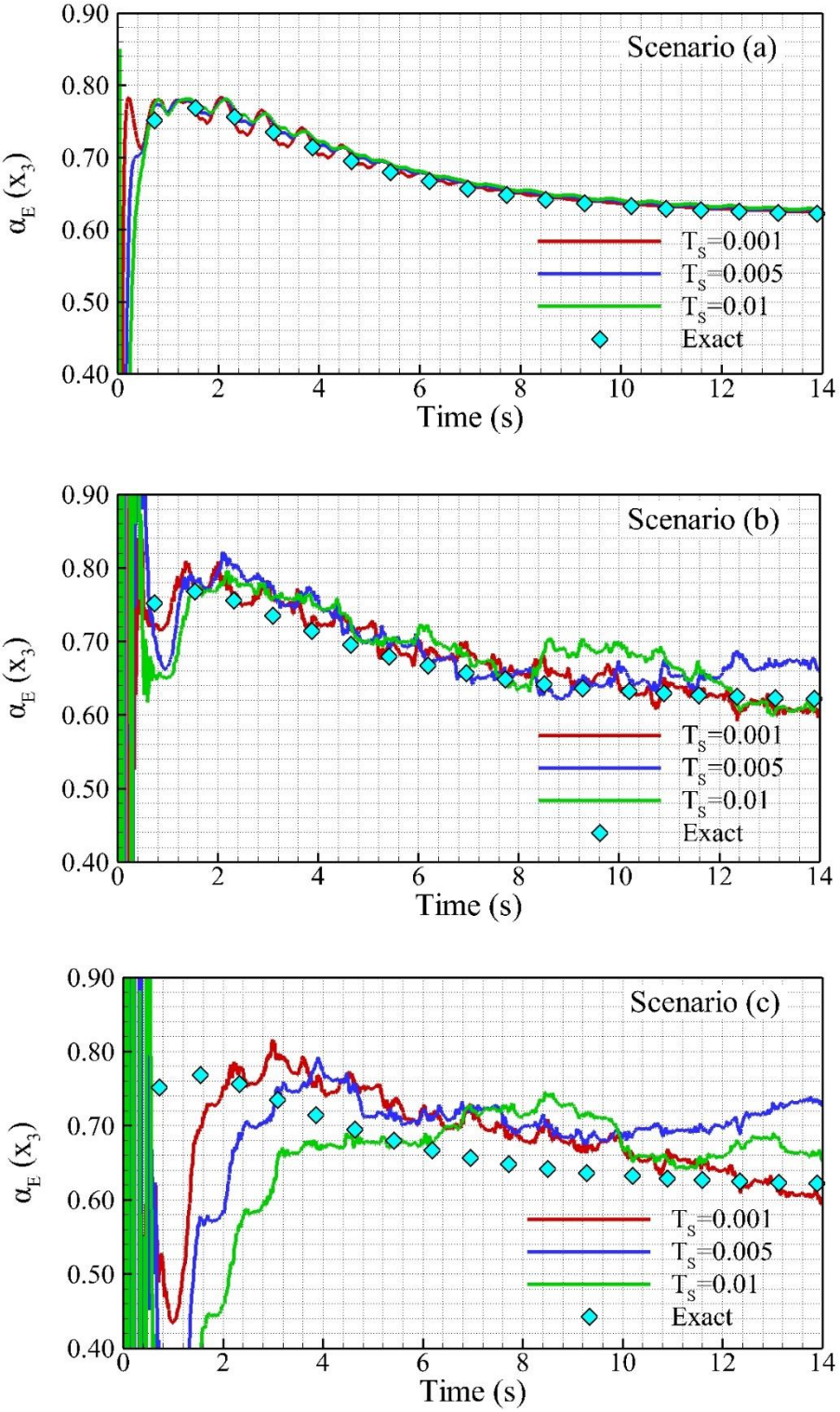

Figure 15. The effects of the sampling time, T_S, on the estimated value of equivalent linear damping coefficient (α_E)

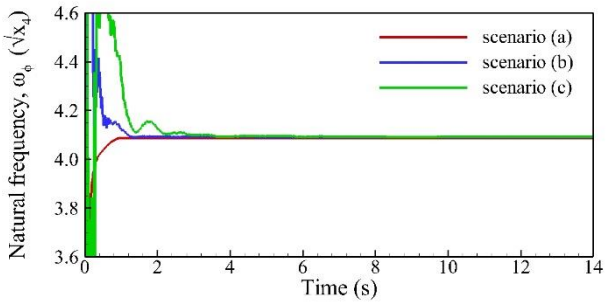

Figure 16. The estimated value of natural frequency (ω_ϕ) at $T_S = 0.01\ s$

Tables

Table 1. Hydrostatic properties of the DTMB hull model 5512

Symbol	Unit	Model 5512
L	*m*	3.048
B	*m*	0.405
T	*m*	0.132
S_W	m^2	1.459
C_B	-	0.506
LCG	*m*	1.536
VCG	*m*	0.030
k_φ	*m*	0.158
T_φ	*s*	1.540
GM	*m*	0.043

Table 2. Simulation parameters

Coefficients	a	b	c	α	β	γ

	0.2363	0.0202	-0.0017	0.3092	0.8680	-1.1524

Table 3. The numerical peaks of the roll response

i	0	1	2	3	4	5	6	7	8	9
ϕ (deg)	10	7.504	5.562	4.130	3.090	2.332	1.774	1.359	1.047	0.810
ϕ_m (deg)	8.752	6.533	4.846	3.610	2.711	2.053	1.567	1.203	0.929	0.720
$\Delta\phi$ (deg)	2.496	1.942	1.432	1.040	0.758	0.558	0.415	0.312	0.237	0.181
i	10	11	12	13	14	15	16	17	18	19
ϕ (deg)	0.629	0.490	0.383	0.299	0.235	0.184	0.144	0.113	0.089	0.070
ϕ_m (deg)	0.560	0.437	0.341	0.267	0.210	0.164	0.129	0.101	0.080	0.063
$\Delta\phi$ (deg)	0.139	0.107	0.084	0.064	0.051	0.040	0.031	0.024	0.019	0.015

Table 4. Comparison of the decay and extinction coefficients

Coefficients	a	b	c	α	β	γ
Target values	0.2363	0.0202	-0.0017	0.3092	0.8680	-1.1524
Estimated	0.2377	0.0200	-0.0017	0.3086	0.8594	-1.1613
Difference*	0.59 %	0.99 %	0.00 %	0.19 %	0.99 %	0.77 %

*$\text{Difference} = \frac{(\text{Exact} - \text{Estimated})}{\text{Exact}}$

Table 5. RMSE values for the first state for various choices of σ_{p3} in EKF(s)

Scenario	RMSE (deg)		
	σ_{p1}	σ_{p2}	σ_{p3}
Scenario (a)	$3.28\text{x}10^{-5}$	$2.01\text{x}10^{-5}$	$1.11\text{x}10^{-5}$
Scenario (b)	$2.70\text{x}10^{-2}$	$2.68\text{x}10^{-2}$	$2.67\text{x}10^{-2}$
Scenario (c)	$1.36\ \text{x}10^{-1}$	$1.35\ \text{x}10^{-1}$	$1.34\ \text{x}10^{-1}$

Author Biography

Yavuz Hakan Ozdemir received his BSc degree in Naval Architecture and Marine Engineering from Yildiz Technical University, Istanbul, Turkey, in 2005. He then pursued his MSc and PhD degrees in Naval Architecture and Marine Engineering from the same university, graduating in 2007 and 2014, respectively. In 2017, he joined the Department of Motor Vehicles and Transportation Technologies as

an Assistant Professor. Dr. Ozdemir's interests include Ship Hydrodynamics, Fluid Mechanics, and Mathematical Programming. He has published numerous valuable articles on these topics in various scientific journals.